Wideband Triangular-Cavity-Cascaded Antennas

Le Chang, *Student Member, IEEE*, Zhijun Zhang, *Fellow, IEEE*, Yue Li, *Member, IEEE*, and Zhenghe Feng, *Fellow, IEEE*

***Abstract*— A triangular-cavity-cascaded antenna is proposed and analyzed for wideband applications. By alternatively and periodically shorting a metallic plate on its edges with small slices, isosceles-triangular field patterns are generated and cascaded for wideband antenna design. Synchronous electric edge fields which contribute to radiation occupy almost all the areas of both sides of the plate. Compared with a typical microstrip antenna with a rectangular cavity, the triangular-cavity-cascaded antenna is a relatively open structure with less shorting boundary around. As a result, the quality factor is smaller, and the impedance bandwidth is wider. In order to prove the design strategy, a 1-D cascaded antenna with 1 × 5 triangular cavities and a 2-D cascaded antenna with 2 × 5 triangular cavities are fabricated and tested. Experimental results show that the impedance bandwidths of 1-D and 2-D antennas are 35.66% and 21.43%, while the peak gains are 13.27 and 16.47 dBi, respectively.**

***Index Terms*— Cavity-cascaded antenna, dielectric resonator antenna (DRA), Fabry–Perot (FP) cavity, rectangular cavity, triangular cavity.**

I. Introduction

RESONANT cavity antennas are widely used in modern telecommunication and radar systems due to their directional beams. Radiation analysis of a rectangular parallel-plate structure (patch structure) based on cavity model was detailed in [1]. Microstrip antenna arrays can be viewed as cavity antenna arrays. They have the merits of low profile, light weight, and easy integration with other components. The parallel-fed and series–parallel-fed microstrip arrays are most widely used. A 16×16 aperture-coupled parallel-fed microstrip planar array operating at 35 GHz was introduced in [2]. Asymmetrical feed networks were adopted to achieve uniform electric current intensity for each element, and U slot was embedded into each element to enhance operating bandwidth [3]. Fabry–Perot (FP) cavity antenna is a half-wavelength height resonant cavity formed by a reflecting screen and a partially reflecting sheet (PRS) [4]. The primary radiator, such as patch, slot, open waveguide [4]–[10], or antenna array [11], can be used as the feeding source. Perforated or wire grids [4]–[6], periodic dipoles [7], artificial magnetic conductor (AMC), or electromagnetic bandgap superstrate [8]–[11] can be used as the PRS. Some methods were put forward to lower the profile of the Fabry-Perot cavity antennas. AMC was applied as either of the two metallic reflectors to halve the traditional FP antenna height [8]. Dielectric-filled effect further decreased the height to one-ninth wavelength [9]. Both the reflecting screen and PRS constructed by AMC structures lowered the profile to 1/60th wavelength [10]. Dielectric resonator antennas (DRAs) are high-efficiency cavity antennas. A systematic study on DRAs was first presented in [12]. Since then, DRAs with various shapes, such as rectangular [13], spherical [14], triangular [15], and annular [16], and different feeding methods, such as probe fed [17], microstrip line fed [18], coplanar waveguide fed [19], and aperture fed [15], have been investigated. Several rigorous numerical analysis methods [20], [21] together with experimental results [22], [23] have been conducted to evaluate the resonant frequencies, Q-factors, and model field distributions of the cylindrical resonant antennas.

Other cavity antennas explored by scholars were published as well. In [24], by using the 1-order and 3-order modes of an open cavity, a dual-band ultrathin cavity antenna achieved 12.5% and 20.5% tunable bandwidths for the low and high bands, respectively. Two electrically large circular-polarized metallic cavity antennas with a common average gain of 8.5 dBi for satellite applications were presented in [25] and [26]. A high-impedance ground plane was used to improve the pattern of the circular open waveguide [27]. Diffraction analysis of a rectangular open-ended cavity was reported in [28]. By stacking a two-end-open gate-shaped cavity on a single-end-open rectangular cavity, a switched-beam antenna with unidirectional pattern was achieved [29]. Four beam-switched planar pattern diversity arrays were obtained by using four trapezoidal cavities and two 3-dB hybrid couplers [30], [31]. Two 2 × 2 millimeter-wave substrate integrated waveguide (SIW) slotted narrow-wall fed cavity antenna arrays featuring wideband performances (about 12%) were introduced in [32]. An SIW-fed 60-GHz cavity array fabricated using multilayered low-temperature cofired ceramic technology with a bandwidth of 17.1% and peak gain of 22.1 dBi was reported in [33].

Rectangular-cavity-cascaded antennas based on the TM_{1n0} ($n = 0.5$) mode were proposed in [34] and [35]. By using the N-order mode of the N-unit cavity antenna, fan-shaped beams with impedance bandwidths of 11.78% and 12.15% were achieved. In this paper, a 1-D cascaded antenna with a triangular cavity is proposed. By alternatively and periodically shorting a metallic plate on its edges with small

Manuscript received November 25, 2015; revised March 10, 2016; accepted April 26, 2016. Date of publication April 29, 2016; date of current version July 5, 2016. This work was supported in part by the National Basic Research Program of China under Contract 2013CB329002, in part by the National Natural Science Foundation of China under Contract 61525104, and in part by the China Post-Doctoral Science Foundation under Project 2015T80084.

The authors are with the State Key Laboratory on Microwave and Communications and the Tsinghua National Laboratory for Information Science and Technology, Tsinghua University, Beijing 100084, China (e-mail: changle4015@126.com; zjzh@tsinghua.edu.cn; lyee@tsinghua.edu.cn; fzh-dee@tsinghua.edu.cn).

Color versions of one or more of the figures in this paper are available online at http://ieeexplore.ieee.org.

Digital Object Identifier 10.1109/TAP.2016.2560946

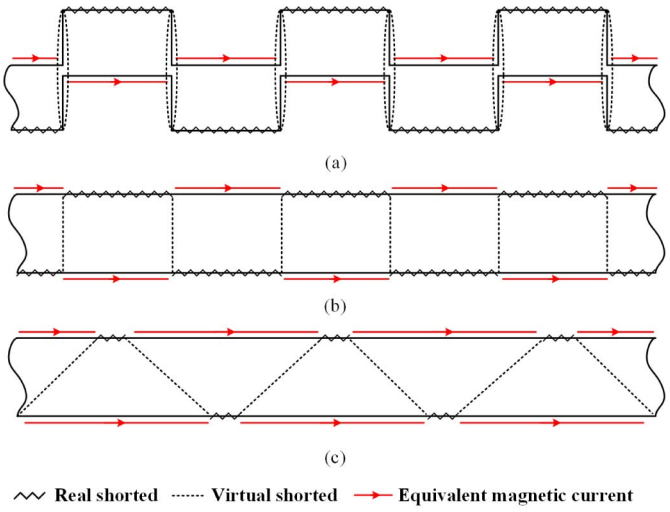

Fig. 1. Rectangular-cavity-cascaded antenna topologies in (a) [34] and (b) [35]. (c) Triangular-cavity-cascaded antenna topology. (The topologies illustrate the top view of antennas and the ground planes are omitted.)

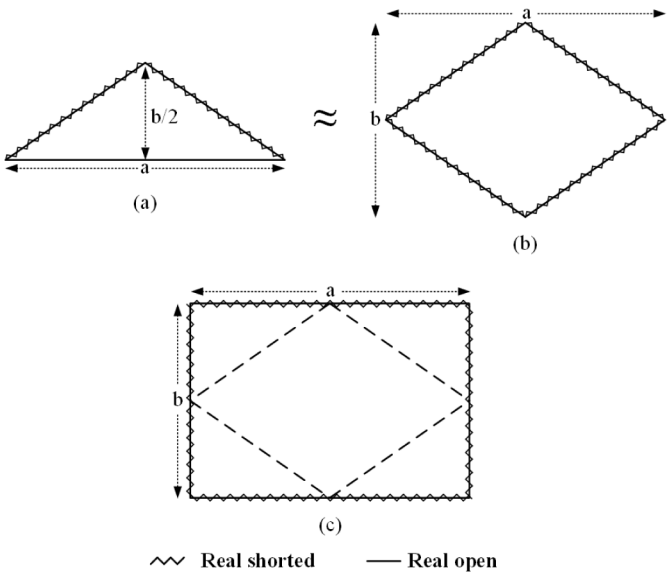

Fig. 2. (a) Isosceles-triangular open cavity antenna. (b) Rhomboid cavity resonator formed by two isosceles-triangular cavity resonators. (c) Rectangular cavity resonator enclosing the rhomboid cavity resonator.

slices, and selecting proper dimensions of the plate and slices, cascaded triangular field patterns are engineered for wideband antenna design. Synchronous electric edge fields which contribute to radiation cover almost both sides of the plate everywhere. Therefore, the triangular-cavity-cascaded antenna is a relatively open structure with less shorting boundary around compared to antennas composed of a rectangular cavity, leading to a smaller quality factor, and as a result, the impedance bandwidth is wider. The fabricated 1×5 triangular-cavity-cascaded antenna prototype shows a bandwidth of 35.66%, which is almost tripled compared to the rectangular-cavity-cascaded antennas [34], [35]. Moreover, the proposed 1-D antenna has the merit of being scalable along one direction to achieve a broadside directivity surpassing 16 dBi. A 2-D triangular-cavity-cascaded antenna is also designed and fabricated to improve the antenna gain. The measured bandwidth is 21.43% and the peak gain is 3.2 dB higher than that of the 1-D antenna.

II. Triangular-Cavity-Cascaded Topology

The antenna topology comparison based on the rectangular and triangular open cavities is illustrated in Fig. 1. The antenna topology in [34] is depicted in Fig. 1(a), the rectangular open cavities are cascaded alternatively and integrated into a whole. For fabrication convenience, the topology can be evolved to what Fig. 1(b) shows [35]. By alternatively and periodically shorting a rectangular metallic plate on its edges with a number of identical end-to-end walls, a more compact structure is established. The equivalent radiating magnetic currents occupy half the area of the two sides. If the length of the shorting walls decrease, the radiating aperture enlarges. As shown in Fig. 1(c), if the lengths of these shorting walls are small enough, virtual shorted circuits can be formed along the tilted line segments between the adjacent shorting slices. So, isosceles-triangular open cavities are cascaded alternatively, and the radiating magnetic currents cover almost all the areas of the two sides, leading to a nearly doubled radiating aperture compared to the rectangular cavity antenna case [34], [35]. Therefore, the triangular-cavity-cascaded antenna is a relatively open structure with less shorting boundary around. As a result, the quality factor is smaller, and the impedance bandwidth is wider.

An analytical solution for the triangular resonator has been detailed in [36] and [37]. Here, we solve the isosceles-triangular open cavity antenna in a straight way for easy understanding. In [30], the resonant condition of the trapezoidal cavity was estimated roughly through the rectangular cavity. In this part, the resonant frequency of an isosceles-triangular open cavity is deduced from the rhomboid cavity enclosing it. The operating frequency of the isosceles-triangular open cavity antenna is shown in Fig. 2(a) with the bottom length of a and midperpendicular length of $b/2$ approximately equal to the fundamental eigenfrequency of the rhomboid cavity resonator, as shown in Fig. 2(b). Without considering the fringing effect, their frequencies should be completely the same. The latter can be evaluated with the help of the rectangular cavity resonator that encloses the rhomboid cavity, as depicted in Fig. 2(c). Rectangular cavity resonators have an explicit analytical solution for their dominant mode

$$f_{\text{rect}} = \frac{c}{2} \times \sqrt{\left(\frac{1}{a}\right)^2 + \left(\frac{1}{b}\right)^2} \tag{1}$$

where c denotes the light velocity in free space. We intuitively conceive the difference between the frequencies of the rectangular and rhomboid cavity resonators to be a coefficient, which is closely related to the rectangular cavity aspect ratio (b/a)

$$f_{\text{rhom}} = C_{b/a} \times f_{\text{rect}}. \tag{2}$$

Resonant frequencies of the rectangular and rhomboid cavity resonators are solved using the *Eigenmode* solution type of the full-wave electromagnetic solver Ansoft HFSS. As shown

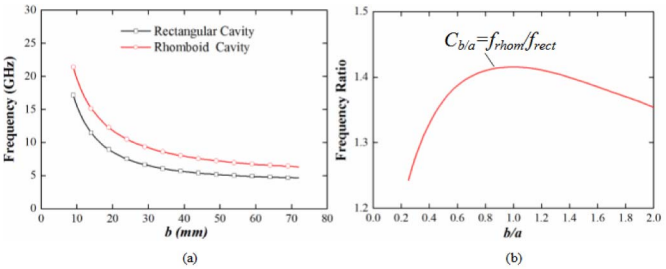

Fig. 3. (a) Resonant frequencies of the rectangular and rhomboid cavity resonators inside the former varying with rectangular cavity width while its length is fixed at 36 mm. (b) Frequency ratio at different rectangular cavity aspect ratios.

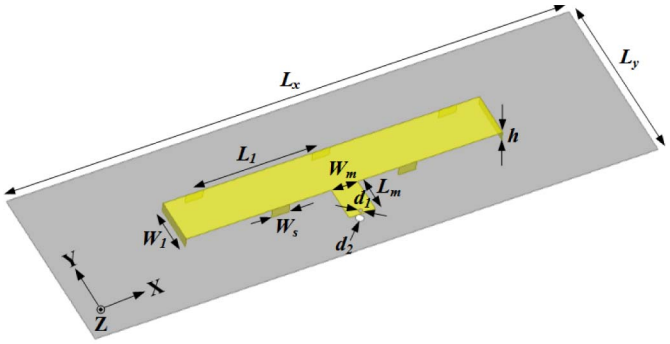

Fig. 4. Geometry of the proposed 1-D triangular-cavity-cascaded antenna.

in Fig. 3(a), these two curves are obtained by varying b from 5 to 72 mm while fixing $a = 36$ mm, which means that the aspect ratio maintains a reasonable value varying from 1:4 to 2:1. Further decreasing or increasing b will cause the realistic cavity resonator hard to excite. As can be seen, the frequency of the rhomboid cavity resonator is higher than that of the rectangular cavity and they are both inversely proportional to b. The coefficient is obtained by dividing one by the other, and the result is illustrated in Fig. 3(b). It is worth mentioning that this is a universal solution for the rhomboid cavity resonator. Considering the fringing effect, the realistic frequency is lower. A detailed design guideline based on this part is given in Section III.

III. 1-D Triangular-Cavity-Cascaded Antenna

A. 1-D Antenna Geometry

In this paper, a five-unit 1-D triangular-cavity-cascaded antenna is taken as an example, as shown in Fig. 4. Five shorting slices are evenly distributed underneath a two-end-shorted rectangular metallic plate and located on its edges alternatively. The two shorted circuits at the head and tail aim to obtain a pure field distribution. The dimensions of the metallic plate are 90 mm × 13 mm × 3 mm. The width of each shorting slice is 5 mm and the interelement spacing is 36 mm. The five slices divide the 1-D antenna into three identical triangular open cavities and two right-trapezoid open cavities. The proposed 1-D antenna is fed from the open edge of the center cavity by using a microstrip line whose width and length are 7.5 and 10 mm, respectively. Commercially available KFDS96-12 SMA connector with a center conductor

TABLE I
Detailed Dimensions of the Proposed 1-D Antenna

Parameter	L_x	L_y	L_1	W_1	h
Value(mm)	160	50	36	13	3
Parameter	W_s	L_m	W_m	d_1	d_2
Value(mm)	5	10	7.5	1.2	2.2

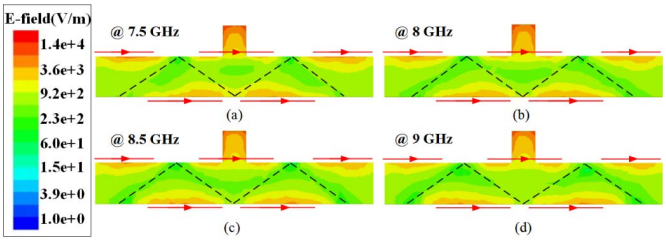

Fig. 5. Complex electric field distributions at (a) 7.5, (b) 8, (c) 8.5, and (d) 9 GHz. Red arrow lines: equivalent currents. Black dashed lines: virtual shorted circuits.

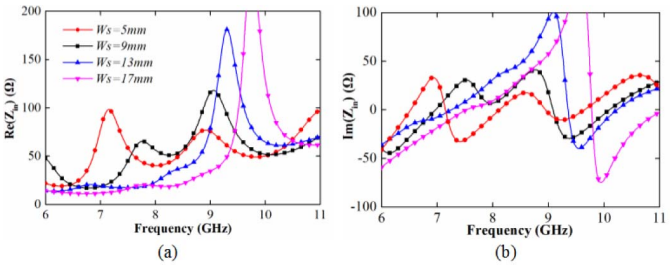

Fig. 6. (a) Real and (b) imaginary parts of input impedances at different shorting slice widths.

diameter of 1.2 mm is used for feeding. The ground plane with dimensions of 160 mm × 50 mm has been optimized to obtain the maximum broadside gain. Detailed dimensions are listed in Table I.

B. Field Distributions and Input Impedance

The electric field distributions at four frequency points are depicted in Fig. 5. The triangular field modes are shown clearly by using the dashed lines which denote virtual shorted circuits. The field distributions of the three triangular open cavities in the middle are becoming more and more like the triangular pattern as the frequency increases from 7.5 to 8.5 GHz. At 8.5 GHz, the distribution is the most pure triangular pattern. As the frequency increases further to 9 GHz, the field pattern starts to get worse. Above 9 GHz, the field patterns are desultory. Thus, the electric field distribution maintains a proper triangular form in the frequency band approximately from 7.5 to 9 GHz, so a flat gain curve is expected in this band.

Since the desired field distribution can be maintained between 7.5 and 9 GHz, the impedances in this band should be matched as well. The width of the shorting slices is a significant parameter affecting the input impedance. Fig. 6 shows the real and imaginary parts of the input impedance at different slices widths. The real and imaginary parts both become more and more flat as the length decreases from 17 to 5 mm. In the frequency band from 7.5 to 9 GHz, the real part fluctuates

TABLE II

DIRECTIVITY AT 8.5 GHz VARYING WITH THE CAVITY NUMBER OF THE PROPOSED 1-D ANTENNA

Cavity Number	1	3	5	7
Directivity/dBi	7.73	11.34	13.45	14.48
Cavity Number	9	11	13	15
Directivity/dBi	15.11	15.64	15.98	16.33

around 50 Ω and the imaginary part around 0 Ω when the width is 5 mm. Therefore, the width of 5 mm is selected to achieve a relatively wide bandwidth.

C. Scalability

The proposed 1-D antenna has the merit of being scalable along the X direction to achieve more gains. Directivity at 8.5 GHz varying with the radiating cavity number is shown in Table II. A common ground plane with dimensions of 300 mm $\times$ 50 mm is used here. As can be seen, the energy can spread to a long distance underneath the plate to achieve a large aperture, and the available broadside directivity can exceed 16 dBi.

D. Design Guideline

The core of determining antenna parameters is the relationship between the operation frequency of the rhomboid and rectangular cavity resonators [Fig. 3(b)]. The design procedure is summarized in this section.

First, the antenna shape which is indicated by the aspect ratio $L_1/(2W_1)$ is chosen according to the optimized field distribution at center frequency. If the antenna shape is presented as narrow and long, the two cavities at the two ends may be coupled with weak energy; if it is presented as wide and short, only three effective triangular field modes exist. Through numerous studies, it is found that the proper ratio lies between 0.6 and 1.9. The antennas defined by this aspect ratio value have ideal broadside directivity.

1) Selecting the aspect ratio $L_1/(2W_1)$ of the triangular-cavity-cascaded antenna as between 0.6 and 1.9, and once the ratio is chosen, the coefficient $C_{b/a}$ is determined.
2) According to the frequency relation formula (2), the resonant frequency of the corresponding rectangular cavity is obtained by dividing the coefficient $C_{b/a}$ by the desired frequency of the triangular-cavity-cascaded antenna. Then, by using the rectangular cavity resonant frequency formula (1), the initial values of L_1 and W_1 together with the antenna height h are selected.
3) The initial width (W_s) of the shorting slice is selected, which is far smaller than the value of L_1.
4) The values of L_1 and W_1 are fine tuned to obtain the most uniform field distribution at center frequency, and then the value of W_s is fine tuned to obtain the widest achievable impedance bandwidth.
5) Based on the edge impedance, proper length (L_m) and width (W_m) of the feeding microstrip line are selected for impedance matching.

E. Simulation and Measured Results

The prototype of the proposed 1-D triangular-cavity-cascaded antenna is shown in Fig. 7, which is fabricated by two pieces of 0.5-mm-thick copper plates. The cost is less than U.S. $2. Fig. 8(a) shows the measured reflection coefficient in comparison with the simulated result in the frequency band from 4 to 15 GHz. The measured result agrees well with the simulation. Five resonant frequency points, which are the 1-, 3-, 5-, 7-, and 9-order modes, are observed [34], [35]. The simulated bandwidth is 34.54% from 7.4 to 10.49 GHz, while the measured bandwidth is 35.66% from 7.19 to 10.31 GHz. Bandwidth comparison of the proposed antenna with microstrip arrays, SIW slot antennas, and metallic slotted waveguide antennas is listed in Table III. The profiles of these reference antennas are comparable with or higher than that of the proposed antenna. It is shown that the proposed antenna has the merit of a relatively wide bandwidth.

Fig. 5(b) shows the simulated and measured broadside gains. The simulated gains are up to 13.40 dBi at 8.4 GHz with

TABLE III

COMPARISON OF THE PROPOSED 1-D ANTENNA WITH OTHER ANTENNAS

Antennas	h (λ_L)	Bandwidth
[2]	0.07	8%
[3]	0.06	3×2 array:17.66% 3×3 array:19.72%
[39]	0.06~0.07	E-plane spare array: 13.7% H-plane spare array: 9.7%
[40]	0.07	5.97%
[41]	0.34	14.63%
[42]	0.29	20.69%
[43]	~0.5	16%
Proposed	0.07	35.66%

λ_L is the free space wavelength referring to the lowest frequency.

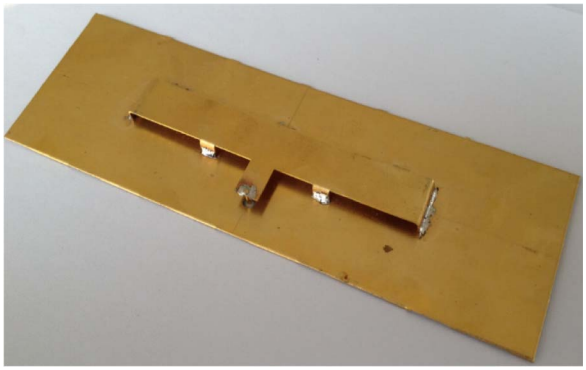

Fig. 7. Prototype of the proposed 1-D triangular-cavity-cascaded antenna.

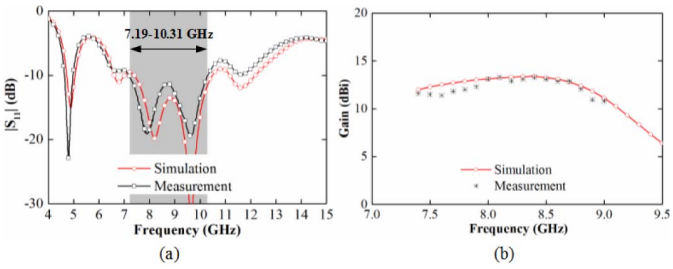

Fig. 8. Simulated and measured (a) reflection coefficients and (b) broadside gains of the proposed 1-D antenna.

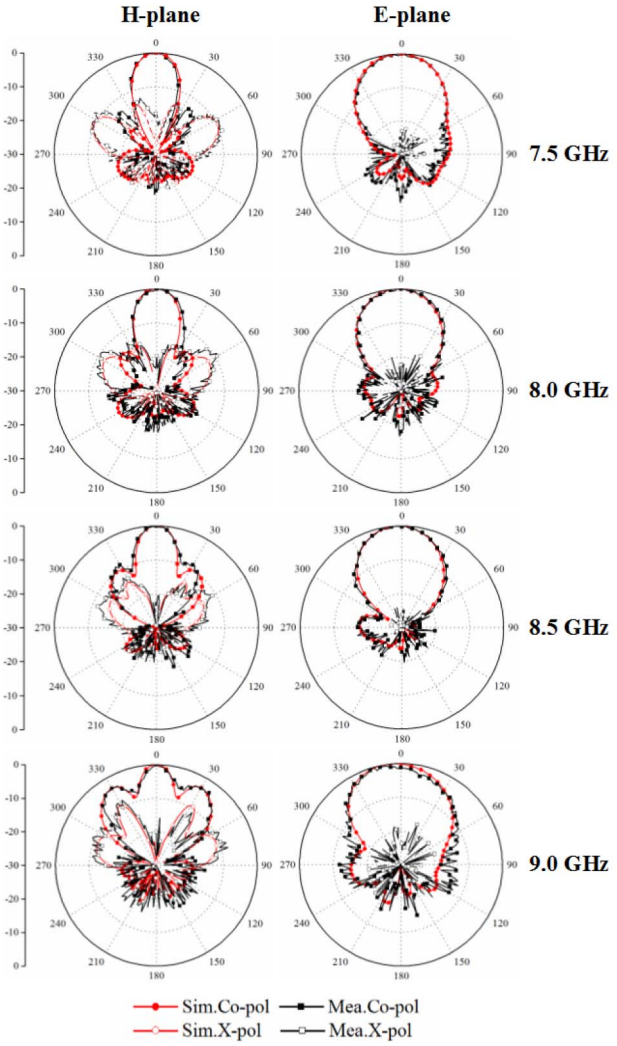

Fig. 9. Simulated and measured normalized patterns in two principal planes of the proposed 1-D antenna at 7.5, 8, 8.5, and 9 GHz.

a 3-dB gain bandwidth of 20.61% in the frequency range 7.4–9.1 GHz while the measured gains are up to 13.27 dBi at 8.4 GHz with a 3-dB gain bandwidth of 22.36% in the frequency range 7.19–9 GHz. (Limited by the microwave anechoic chamber in our laboratory, the gains and patterns can be measured up to 9 GHz.) Among the 3-dB gain bandwidths, the simulated total efficiency is higher than 90.77%.

Fig. 9 shows the simulated and measured normalized radiation patterns in two principal planes at 7.5, 8, 8.5, and 9 GHz. Fan-shaped beams are observed. The simulated and measured 3-dB beam widths and cross-pol levels in H- and E-plane are listed in Table IV. The measurement agrees well with the simulation. The patterns are stable between 7.5 and 8.5 GHz, and the measured first side lobe levels (FSLLs) in the H-plane are −13.11, −16.43, and −8.40 dB at 7.5, 8, and 8.5 GHz, respectively. At 9 GHz, the FSLL in H-plane is as high as −3.47 dB, and the beam widths get wider in both principal planes. The cross-pol levels in the E-plane are much lower than that of the H-plane. It is caused because the structure is symmetrical about the E-plane while asymmetrical about the H-plane, so the cross-polarized

TABLE IV
SIMULATED AND MEASURED BEAM WIDTHS AND CROSS-POL LEVELS OF THE PROPOSED 1-D ANTENNA

	Frequency (GHz)	H-plane		E-plane	
		Simulated	Measured	Simulated	Measured
3-dB Beam widths (degree)	7.5	24	24	44	46
	8.0	24	26	44	44
	8.5	20	22	42	42
	9.0	17	16	54	50
X-pol Levels (dB)	7.5	-9.53	-8.06	-42.70	-22.08
	8.0	-12.30	-9.12	-43.23	-18.25
	8.5	-14.23	-11.08	-41.38	-22.56
	9.0	-9.13	-8.03	-41.39	-17.12

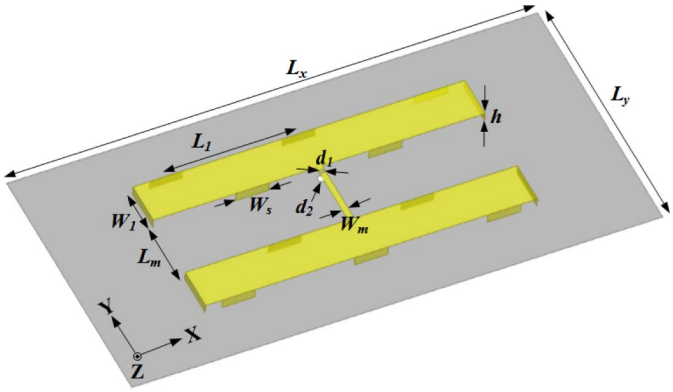

Fig. 10. Geometry of the proposed 2-D triangular-cavity-cascaded antenna.

fields interfere destructively everywhere in the E-plane. However, in some directions in the H-plane, the cross-polarized fields interfere constructively. Furthermore, parasitic radiation from the feeding microstrip line deteriorates the cross-pol.

IV. 2-D TRIANGULAR-CAVITY-CASCADED ANTENNA

In order to improve the antenna gain, a 2×5 2-D antenna is built. Two 1-D antennas are connected with each other by using a microstrip line whose length is $0.6\lambda_0$ (λ_0 is the wavelength of the center frequency) for high gain and avoiding grating lobe or high side lobe level (SLL). The simple offset feeding approach is adopted to provide the required 180° phase difference. Such a frequency-dependent feeding approach cannot offer perfect reversed phases in the 1-D antenna band, so the feeding location is selected according to the best gain curve. By sacrificing the bandwidth, a compact triangular-cavity-cascaded 2-D antenna is constructed.

The geometry of the proposed 2-D antenna is shown in Fig. 10. Five parameters are distinct from the 1-D case, while the rest remain unchanged. The spacing (L_1) and width (W_s) of the shorting slices, the length (L_m) and width (W_m) of the feeding microstrip line, and the width (L_y) of the ground plane are revised to 40 and 10, 20.5 and 1.8, and 80 mm, respectively. Detailed dimensions are listed in Table V. Fig. 11 shows the prototype, whose cost is also less than U.S. $2.

Fig. 12(a) shows the measured reflection coefficient in comparison with the simulated result in the frequency band from 4 to 15 GHz. The measured result agrees well with

TABLE V

DETAILED DIMENSIONS OF THE PROPOSED 2-D ANTENNA

Parameter	L_x	L_y	L_1	W_1	h
Value*(mm)*	*160*	*80*	*40*	*13*	*3*
Parameter	W_s	L_m	W_m	d_1	d_2
Value*(mm)*	*10*	*20.5*	*1.8*	*1.2*	*2.2*

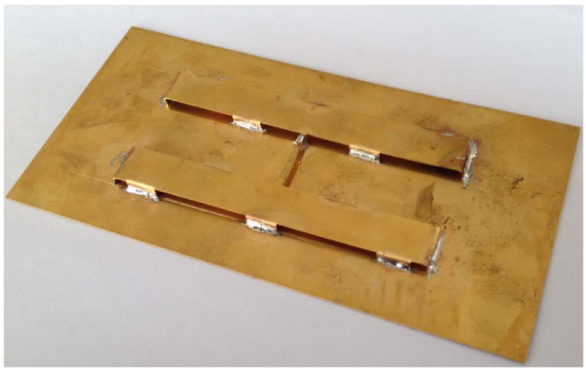

Fig. 11. Prototype of the proposed 2-D triangular-cavity-cascaded antenna.

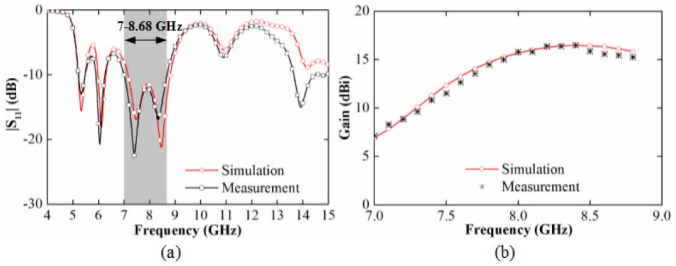

Fig. 12. Simulated and measured (a) reflection coefficients and (b) broadside gains of the proposed 2-D antenna.

the simulation. The simulated bandwidth is 20.55% in the frequency range 7.16–8.8 GHz, while the measured bandwidth is 21.43% in the frequency range 7–8.68 GHz. The bandwidth is decreased compared with the 1-D antenna: the simple offset feeding approach causes the electrical lengths from the feeding location to the two 1-D antennas to be different at different frequency points, leading to different matching conditions of the two 1-D antennas. However, it is still a relatively wide bandwidth.

Fig. 12(b) shows the simulated and measured broadside gains. Good agreement is observed. The simulated and measured maximum gains are both 16.47 dBi at 8.4 GHz and their 3-dB gain bandwidths are both 13.33% in the frequency range 7.7–8.8 GHz. The maximum gain is 3.2 dB higher than that of the 1-D antenna. Among the 3-dB gain bandwidths, the simulated radiation efficiency is higher than 89.65%.

Fig. 13 shows the simulated and measured normalized radiation patterns in two principal planes at 7.2, 7.6, 8, and 8.4 GHz, respectively. Pencil-shaped beams are observed. The simulated and measured 3-dB beam widths, FSLLs, and cross-pol levels in the H- and E-plane are listed in Table VI. The measurement agrees well with the simulation. At 7.2 GHz, the broadside gain is relatively small and there exists a high FSLL. The patterns are good and stable around the

TABLE VI

SIMULATED AND MEASURED BEAM WIDTHS, FSLLS, AND CROSS-POL LEVELS OF THE PROPOSED 2-D ANTENNA

	Frequency (GHz)	H-plane		E-plane	
		Simulated	Measured	Simulated	Measured
3-dB Beam widths (Degree)	7.2	20	20	34	30
	7.6	20	20	28	26
	8.0	18	19	26	25
	8.4	18	19	26	24
FSLLs (dB)	7.2	-5.58	-5.22	-11.42	-7.80
	7.6	-9.14	-7.95	-14.52	-11.07
	8.0	-11.50	-10.07	-14.58	-12.59
	8.4	-12.28	-11.71	-13.10	-12.93
X-pol Levels (dB)	7.2	-11.01	-9.14	-34.94	-18.96
	7.6	-15.29	-11.75	-44.89	-21.82
	8.0	-21.06	-16.46	-48.35	-24.89
	8.4	-20.61	-18.14	-46.14	-23.94

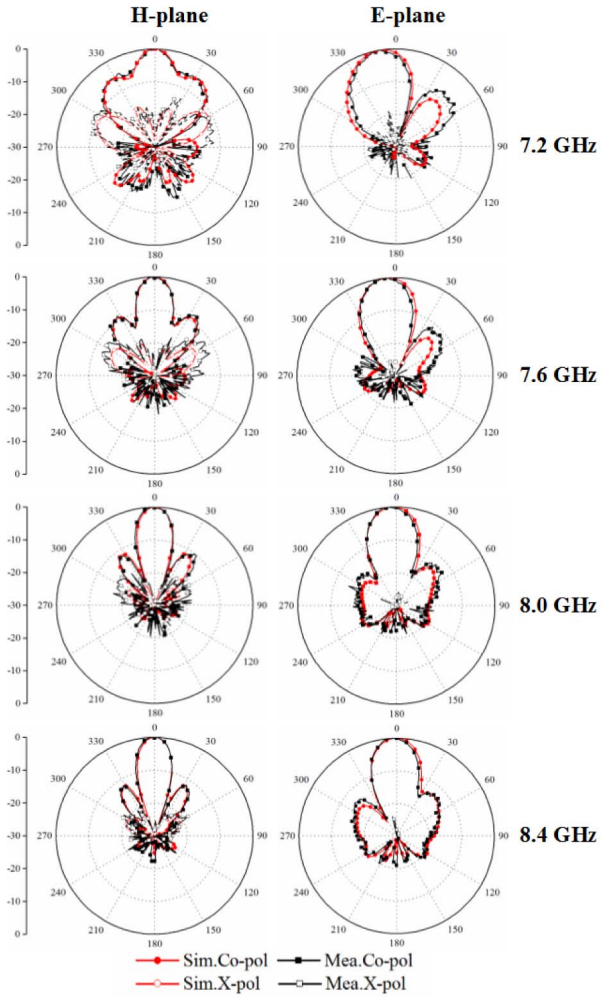

Fig. 13. Simulated and measured normalized patterns in two principal planes of the proposed 2-D antenna at 7.2, 7.6, 8, and 8.4 GHz.

5-order mode frequency range at 7.6, 8, and 8.4 GHz. The measured broadside gains are higher than 12.64 dBi and the FSLLs are smaller than −7.95 dB in both E-plane and H-plane when the operating frequencies are above 7.6 GHz. The cross-pol levels in the E-plane are much lower than that of the H-plane as mentioned above. Compared with the 1-D antenna case, the cross-pol levels are improved, attributing

to the fact that the reversed excitation phases of the two feeding mircrostrip lines make their parasitic radiation to cancel out.

V. Conclusion

Based on the triangular cavity, a five-unit 1-D cavity cascaded antenna is constructed. Triangular open cavities are cascaded alternatively and integrated underneath the metallic plate, resulting in a rather compact structure, which can be fabricated easily. All the edge fields beside the metallic plate are in-phase and occupy almost all the area of the two sides, forming an open structure, lowering the quality factor and, as a result, wide bandwidth performance is achieved. By using a single probe fed, the proposed 1-D antenna can be extended to acquire a gain of over 16 dBi. A 1×5 1-D antenna and a 2×5 2-D triangular-cavity-cascaded antenna with impedance bandwidths of 35.66% and 21.43% and peak gains of 13.27 and 16.47 dBi, respectively, are fabricated. Due to the all-metal structures, the proposed antennas have the merits of low cost and light weight, and are especially useful in applications where dielectrics are problematic, such as space applications.

References

[1] M. Leone, "The radiation of a rectangular power-bus structure at multiple cavity-mode resonances," *IEEE Trans. Electromagn. Compat.*, vol. 45, no. 3, pp. 486–492, Aug. 2003.

[2] Y.-C. L. Liu and Y. E. Wang, "A 16×16 ka band aperture-coupled microstrip planar array," in *Proc. IEEE Antennas Propag. Soc. Int. Symp.*, Jun. 2007, pp. 4373–4376.

[3] H.-D. Chen, C.-Y.-D. Sim, J.-Y. Wu, and T.-W. Chiu, "Broadband high-gain microstrip array antennas for WiMAX base station," *IEEE Trans. Antennas Propag.*, vol. 60, no. 8, pp. 3977–3980, Aug. 2012.

[4] G. Von Trentini, "Partially reflecting sheet arrays," *IRE Trans. Antennas Propag.*, vol. 4, pp. 666–671, Oct. 1956.

[5] R. Sauleau, P. Coquet, T. Matsui, and J. Daniel, "A new concept of focusing antennas using plane-parallel Fabry–Perot cavities with nonuniform mirrors," *IEEE Trans. Antennas Propag.*, vol. 51, no. 11, pp. 3171–3175, Nov. 2003.

[6] S. A. Muhammad, R. Sauleau, and H. Legay, "Small-size shielded metallic stacked Fabry–Perot cavity antennas with large bandwidth for space applications," *IEEE Trans. Antennas Propag.*, vol. 60, no. 2, pp. 792–802, Feb. 2012.

[7] A. P. Feresidis and J. C. Vardaxoglou, "High gain planar antenna using optimised partially reflective surfaces," *IEE Proc.-Microw. Antennas Propag.*, vol. 148, no. 6, pp. 345–350, Dec. 2001.

[8] A. P. Feresidis, G. Goussetis, S. Wang, and J. C. Vardaxoglou, "Artificial magnetic conductor surfaces and their application to low-profile high-gain planar antennas," *IEEE Trans. Antennas Propag.*, vol. 53, no. 1, pp. 209–215, Jan. 2005.

[9] Y. Sun, Z. N. Chen, Y. Zhang, H. Chen, and T. S. P. See, "Subwavelength substrate-integrated Fabry–Pérot cavity antennas using artificial magnetic conductor," *IEEE Trans. Antennas Propag.*, vol. 60, no. 1, pp. 30–35, Jan. 2012.

[10] A. Ourir, A. de Lustrac, and J.-M. Lourtioz, "All-metamaterial-based subwavelength cavities (λ/60) for ultrathin directive antennas," *Appl. Phys. Lett.*, vol. 88, pp. 084103-1–084103-3, Feb. 2006.

[11] R. Gardelli, M. Albani, and F. Capolino, "Array thinning by using antennas in a Fabry–Perot cavity for gain enhancement," *IEEE Trans. Antennas Propag.*, vol. 54, no. 7, pp. 1979–1990, Jul. 2006.

[12] S. A. Long, M. W. McAllister, and L. C. Shen, "The resonant cylindrical dielectric cavity antenna," *IEEE Trans. Antennas Propag.*, vol. 31, no. 3, pp. 406–412, May 1983.

[13] M. W. McAllister, S. A. Long, and G. L. Conway, "Rectangular dielectric resonator antenna," *Electron. Lett.*, vol. 19, pp. 218–219, Mar. 1983.

[14] M. W. McAllister and S. A. Long, "Resonant hemispherical dielectric antenna," *Electron. Lett.*, vol. 20, pp. 657–659, Aug. 1984.

[15] A. Ittipiboon, R. K. Mongia, Y. M. M. Antar, P. Bhartia, and M. Cuhaci, "Aperture fed rectangular and triangular dielectric resonators for use as magnetic dipole antennas," *Electron. Lett.*, vol. 29, no. 23, pp. 2001–2002, 1993.

[16] R. K. Mongia, A. Ittipiboon, P. Bhartia, and M. Cuhaci, "Electric-monopole antenna using a dielectric ring resonator," *Electron. Lett.*, vol. 29, pp. 1530–1531, Aug. 1993.

[17] K. W. Leung, K. M. Luk, K. Y. A. Lai, and D. Lin, "Theory and experiment of a coaxial probe fed hemispherical dielectric resonator antenna," *IEEE Trans. Antennas Propag.*, vol. 41, no. 10, pp. 1390–1398, Oct. 1993.

[18] R. A. Kranenburg and S. A. Long, "Microstrip transmission line excitation of dielectric resonator antennas," *Electron. Lett.*, vol. 24, no. 18, pp. 1156–1157, Sep. 1988.

[19] R. A. Kranenburg, S. A. Long, and J. T. Williams, "Coplanar waveguide excitation of dielectric resonator antennas," *IEEE Trans. Antennas Propag.*, vol. 39, no. 1, pp. 119–122, Jan. 1991.

[20] W. Zheng, "Computation of complex resonance frequencies of isolated composite objects," *IEEE Trans. Microw. Theory Techn.*, vol. 37, no. 6, pp. 953–961, Jun. 1989.

[21] J. A. Pereda, L. A. Vielva, A. Vegas, and A. Prieto, "Computation of resonant frequencies and quality factors of open dielectric resonators by a combination of the finite-difference time-domain (FDTD) and Prony's methods," *IEEE Microw. Guided Wave Lett.*, vol. 2, no. 11, pp. 431–433, Nov. 1992.

[22] A. W. Glisson, D. Kajfez, and J. James, "Evaluation of modes in dielectric resonators using a surface integral equation formulation," *IEEE Trans. Microw. Theory Techn.*, vol. 31, no. 12, pp. 1023–1029, Dec. 1983.

[23] R. K. Mongia, C. L. Larose, S. R. Mishra, and P. Bhartia, "Accurate measurement of Q-factors of isolated dielectric resonators," *IEEE Trans. Microw. Theory Techn.*, vol. 42, no. 8, pp. 1463–1467, Aug. 1994.

[24] Y. Zhao, Z. Zhang, and Z. Feng, "A dual-band tunable ultra-thin cavity antenna," *IEEE Antennas Wireless Propag. Lett.*, vol. 10, pp. 717–720, Jul. 2011.

[25] Y. Zhao, Z. Zhang, and Z. Feng, "An electrically large metallic cavity antenna with circular polarization for satellite applications," *IEEE Antennas Wireless Propag. Lett.*, vol. 10, pp. 1461–1464, 2011.

[26] K. Wei, Z. Zhang, Y. Zhao, and Z. Feng, "Design of a ring probe-fed metallic cavity antenna for satellite applications," *IEEE Trans. Antennas Propag.*, vol. 61, no. 9, pp. 4836–4839, Sep. 2013.

[27] G.-H. Zhang, Y.-Q. Fu, C. Zhu, D.-B. Yan, and N.-C. Yuan, "A circular waveguide antenna using high-impedance ground plane," *IEEE Antennas Wireless Propag. Lett.*, vol. 2, pp. 86–88, 2003.

[28] S. Eardprab and C. Phongcharoenpanich, "Diffraction on a rectangular aperture antenna mounted on an open-ended cavity excited by a probe," in *Proc. Int. Symp. Commun. Inf. Technol.*, Oct./Sep. 2006, pp. 779–782.

[29] R. Tamaki, N. Kuga, and H. Arai, "A low-profile switched-beam antenna with rectangular cavity element and stacked gate-shaped element," in *Proc. IEEE AP-S Int. Symp.*, Jul. 2006, pp. 795–798.

[30] N. Kuga and H. Arai, "A four beam-switched planar array antenna for mobile terminals," in *Proc. IEEE AP-S Int. Symp.*, vol. 3. Jun. 1995, pp. 1450–1454.

[31] N. Kuga and H. Arai, "A planar pattern diversity antenna," in *IEEE AP-S Int. Symp.*, Sep. 1996, pp. 365–368.

[32] Y. Zhang, Z. N. Chen, X. Qing, and W. Hong, "Wideband millimeter-wave substrate integrated waveguide slotted narrow-wall fed cavity antennas," *IEEE Trans. Antennas Propag.*, vol. 59, no. 5, pp. 1488–1496, May 2011.

[33] J. Xu, Z. N. Chen, X. Qing, and W. Hong, "Bandwidth enhancement for a 60 GHz substrate integrated waveguide fed cavity array antenna on LTCC," *IEEE Trans. Antennas Propag.*, vol. 59, no. 3, pp. 826–832, Mar. 2011.

[34] L. Chang, Z. Zhang, Y. Li, and Z. Feng, "All-metal antenna array based on microstrip line structure," *IEEE Trans. Antennas Propag.*, vol. 64, no. 1, pp. 351–355, Jan. 2016.

[35] L. Chang, Y. Li, Z. Zhang, and Z. Feng, "Compact all-metallic cavity-cascaded antenna," *Electron. Lett.*, vol. 52, no. 6, pp. 413–414, Mar. 2016.

[36] Y. Akaiwa, "Operation modes of a waveguide Y circulator (short papers)," *IEEE Trans. Microw. Theory Techn.*, vol. 22, no. 11, pp. 954–959, Nov. 1974.

[37] J. Helszajn and D. S. James, "Planar triangular resonators with magnetic walls," *IEEE Trans. Microw. Theory Techn.*, vol. 26, no. 2, pp. 95–100, Feb. 1978.

[38] S.-W. Qu, C. H. Chan, M.-Y. Xia, and Z. Nie, "High-efficiency periodic sparse microstrip array based on mutual coupling," *IEEE Trans. Antennas Propag.*, vol. 61, no. 4, pp. 1963–1969, Apr. 2013.
[39] H. C. Zhao, R. R. Xu, and W. Wu, "Broadband waveguide slot array for SAR," *Electron. Lett.*, vol. 47, no. 2, pp. 76–77, Jan. 2011.
[40] S.-S. Zhong, W. Wang, and X.-L. Liang, "Compact ridge waveguide slot antenna array fed by convex waveguide divider," *Electron. Lett.*, vol. 41, no. 21, pp. 1151–1152, Oct. 2005.
[41] L. Yan, W. Hong, G. Hua, J. Chen, K. Wu, and T. J. Cui, "Simulation and experiment on SIW slot array antennas," *IEEE Microw. Wireless Compon. Lett.*, vol. 14, no. 9, pp. 446–448, Sep. 2004.
[42] M. Ohira, A. Miura, and M. Ueba, "60-GHz wideband substrate-integrated-waveguide slot array using closely spaced elements for planar multisector antenna," *IEEE Trans. Antennas Propag.*, vol. 58, no. 3, pp. 993–998, Mar. 2010.

Le Chang (S'16) received the B.S. degree in electronics and information engineering from Xidian University, Xi'an, China, in 2012. He is currently pursuing the Ph.D. degree in electrical engineering with Tsinghua University, Beijing, China.

His current research interests include antenna design and theory, particularly in cavity antenna arrays, transmitted arrays, and millimeter-wave air-substrate antennas based on microelectromechanical systems fabrication process.

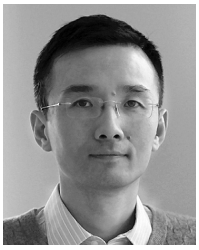

Zhijun Zhang (M'00–SM'04–F'15) received the B.S. and M.S. degrees from the University of Electronic Science and Technology of China, Chengdu, China, in 1992 and 1995, respectively, and the Ph.D. degree from Tsinghua University, Beijing, China, in 1999.

He was a Postdoctoral Fellow with the Department of Electrical Engineering, University of Utah, Salt Lake City, UT, USA, in 1999, where he was appointed as a Research Assistant Professor in 2001. In 2002, he was an Assistant Researcher with the University of Hawaii at Manoa, Honolulu, HI, USA. In 2002, he joined Amphenol T&M Antennas, Lincolnshire, IL, USA, as a Senior Staff Antenna Development Engineer, where he was then promoted to Antenna Engineer Manager. In 2004, he joined Nokia Inc., San Diego, CA, USA, as a Senior Antenna Design Engineer. In 2006, he joined Apple Inc., Cupertino, CA, USA, as a Senior Antenna Design Engineer, where he was then promoted to Principal Antenna Engineer. Since 2007, he has been with Tsinghua University, where he is currently a Professor with the Department of Electronic Engineering. He has authored the book entitled *Antenna Design for Mobile Devices* (Wiley, 2011).

Dr. Zhang served as an Associate Editor of the IEEE TRANSACTIONS ON ANTENNAS AND PROPAGATION from 2010 to 2014, and the *IEEE Antennas and Wireless Propagation Letters* from 2009 to 2015.

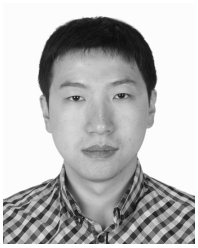

Yue Li (S'11–M'12) received the B.S. degree in telecommunication engineering from Zhejiang University, Hangzhou, China, in 2007, and the Ph.D. degree in electronics engineering from Tsinghua University, Beijing, China, in 2012.

He was a Postdoctoral Fellow with the Department of Electronic Engineering, Tsinghua University, in 2012. In 2013, he was a Research Scholar with the Department of Electrical and Systems Engineering, University of Pennsylvania, Philadelphia, PA, USA. He was also a Visiting Scholar with the Institute for Infocomm Research, Agency for Science, Technology and Research, Singapore, in 2010, and the Hawaii Center of Advanced Communication, University of Hawaii, Honolulu, HI, USA, in 2012. Since 2016, he has been with Tsinghua University, where he is currently an Assistant Professor with the Department of Electronic Engineering. He has authored or co-authored over 60 journal papers and 30 international conference papers, and holds 13 granted Chinese patents. His current research interests include metamaterials, plasmonics, nanocircuits, electromagnetics, mobile and handset antennas, multiple-input and multiple-output and diversity antennas, and millimeter-wave antennas and arrays.

Dr. Li was a recipient of the Young Scientist Awards from the URSI General Assembly in 2014, the Outstanding Doctoral Dissertation of Beijing Municipality in 2013, and the Principal Scholarship of Tsinghua University in 2011.

Zhenghe Feng (M'05–SM'08–F'12) received the B.S. degree in radio and electronics from Tsinghua University, Beijing, China, in 1970.

He has been with Tsinghua University, since 1970, as an Assistant, a Lecture, an Associate Professor, and a Full Professor. His current research interests include numerical techniques and computational electromagnetics, RF and microwave circuits and antenna, wireless communications, smart antenna, and spatial temporal signal processing.